

A Numerical Wave-Structure-Soil Interaction Model with Application to Monolithic Breakwaters Subject to Breaking Wave Impact

H. El Safti & H. Oumeraci

Leichtweiss-Institute for Hydraulic Engineering and Water Resources, Dept. of Hydromechanics and Coastal Engineering, TU Braunschweig, Braunschweig, Germany

ABSTRACT: A one-way CFD-CSD coupled model system is developed within the OpenFOAM® framework to provide a tool for numerical analysis of coastal structures (e.g. vertical breakwaters). This tool is intended to work in parallel with physical experiments to extend the range of testing conditions and give better insight into the processes involved with wave-structure-soil interaction. This numerical tool can be used for optimizing and analyzing innovative coastal structures and designing physical wave-structure-soil interaction experiments. The Computational Structural Dynamics (CSD) model is developed using the finite volume method for the fully dynamic, fully coupled Biot equations. The fully coupled poro-mechanical analysis is handled in a segregated approach in which the skeleton displacement, the pore fluid pressure and the pore fluid velocity (relative to the skeleton) are decoupled at the iteration level. The pore fluid pressure-velocity coupling is resolved using the PISO (Pressure Implicit with Splitting of Operators) algorithm. The u - p approximation is also implemented, which fully neglects the pore fluid acceleration. A frictional contact model is implemented to model soil-structure interaction. A multi-surface plasticity model with the Drucker-Prager failure criterion is introduced to model the behavior of sand foundations under cyclic load posed by wave action on the caisson breakwater (i.e. residual pore pressure build-up and residual deformation). A multiphase Computational Fluid Dynamics (CFD) solver is developed for solving flow inside and outside porous media simultaneously using the principle of volume averaged velocity. A seepage model is implemented to model flow resistance of porous media that includes viscous, transitional, inertial and transient terms. Fluid compressibility is introduced to air as an ideal gas to enhance simulating effect of air entrapment on breaking wave impact.

Keywords: CFD-CSD, OpenFOAM®, Caisson breakwaters, Breaking wave impact, Soil liquefaction, Cyclic mobility

1 INTRODUCTION

Caisson breakwaters are more advantageous compared to rubble mound breakwaters in terms of environmental considerations, quality control, construction speed and multi-purpose use. However, most of the failures experienced by monolithic breakwaters are of geotechnical nature. Despite the extensive research in the past (e.g. Oumeraci et al., 2001 and Kudella et al., 2006), the behaviour of sand foundations underneath monolithic structures, subject to breaking wave impacts, is not fully understood and no reliable numerical model is yet available to reproduce this behaviour. This is partially due to simplifications adopted in the governing equations (i.e. using uncoupled solution or Biot's quasi-static poro-elastic model). Another significant aspect is the selection of a suitable soil constitutive model, which should be able to reproduce with acceptable accuracy salient processes such as the balance between pore pressure generation and dissipation and subsequent soil failure. Only few publications can be found with implementations of non-elastic models. Nevertheless, the implementations do not consider the acceleration of the pore fluid which was proven necessary for the problem at hand (cf. Ülker et al., 2012). A hydrodynamic-geotechnical model system is presented for studying the foundations of marine structures subject to breaking wave impact.

2 THE HYDRODYNAMIC MODEL

The model is implemented in the Eulerian multiphase (Volume-Of-Fluid) solver; *porousInterFoam*. The fluid continuity equation (mass balance) is modified for the incompressible multiphase solver to account for fluid compressibility:

$$\nabla \cdot \bar{\mathbf{U}} + \frac{1}{\rho} \frac{\partial p}{\partial t} = 0 \quad (1)$$

Where the fluid bulk modulus K_f is calculated based on the phase fraction (γ), the degree of saturation ($S_w = V_w/V_v$) and porosity (n) as:

$$\frac{1}{\rho} = \frac{n}{K_f} = n \left(\frac{S_w \gamma}{K_w} + \frac{S_w (1-\gamma)}{K_a} \right) \quad (2)$$

For $K_w = 2200$ MPa is the bulk modulus of pure water, the bulk modulus of air $K_a = p + p_0$; where p is the fluid pressure and $p_0 = 0.101$ MPa is the atmospheric pressure. The porosity and degree of saturation are set to unity outside of the porous zones. The momentum balance is:

$$\rho \left(\frac{(1+c_A)}{n} \frac{\partial \bar{\mathbf{U}}}{\partial t} + \frac{1}{n^2} \bar{\mathbf{U}} \cdot \nabla \bar{\mathbf{U}} \right) = -\nabla p + \frac{1}{n} \left(\nabla \cdot (\boldsymbol{\tau} + \frac{\mathbf{R}}{n}) \right) + \rho \mathbf{b} - \mathbf{S} \quad (3)$$

Where $\bar{\mathbf{U}}$ is the ensemble (Darcy) average velocity ($\bar{\mathbf{U}} = n\mathbf{U}$; where \mathbf{U} is the intrinsic velocity), while (p) is the intrinsic pore pressure, $\rho = \rho_{water}\gamma + (1-\gamma)\rho_{air}$ is the mixture density. \mathbf{S} is a sink term that represents the resistance of the porous media to fluid flow, \mathbf{b} is the body acceleration vector (mostly gravity), $\boldsymbol{\tau} = \mu((\nabla \bar{\mathbf{U}} + (\nabla \bar{\mathbf{U}})^T) - 2/3(\nabla \cdot \bar{\mathbf{U}})\mathbf{I})$ is the deviatoric viscous stress tensor, $\mu = \gamma\mu_{water} + (1-\gamma)\mu_{air}$ is the mixture dynamic viscosity, $\mathbf{R} = \mu_t((\nabla \bar{\mathbf{U}} + (\nabla \bar{\mathbf{U}})^T) - 2/3(\nabla \cdot \bar{\mathbf{U}})\mathbf{I})$ is the additional stress tensor induced by the unresolved turbulence fluctuation (absent for laminar flow), μ_t is the eddy dynamic viscosity, \mathbf{I} is the identity tensor and c_A is the added mass coefficient calculated as $c_A = 0.34(1-n)/n$. The seepage model from Lin and Karunaratna (2007) as explained in Lin (2008) is implemented to calculate the porous media resistance (sink term):

$$I = -\frac{1}{\rho g} \nabla p = \underbrace{\frac{a}{\rho g} \bar{\mathbf{U}}}_{\text{viscous (laminar)}} + \underbrace{c \bar{\mathbf{U}} \sqrt{|\bar{\mathbf{U}}|}}_{\text{(transitional)}} + \underbrace{b \bar{\mathbf{U}} |\bar{\mathbf{U}}|}_{\text{inertial (turbulent)}} + \underbrace{\frac{(1+c_A)}{ng} \frac{\partial \bar{\mathbf{U}}}{\partial t}}_{\text{transient}} \quad (4)$$

$$a = 126 \frac{(1-n)}{n^3} \frac{\nu}{gD_{50}^2}, \quad b = 1.02 \frac{1-n}{n^3} \frac{1}{gD_{50}} \quad \text{and} \quad c = 4.5 \frac{1-n}{n^3} \frac{\nu^{1/2}}{gD_{50}^{3/2}} \quad (5)$$

Where I is the hydraulic gradient a , b and c are constants (ν is the fluid kinematic viscosity and D_{50} is the mean diameter of the porous material). The model incorporates viscous and inertial components (Darcy-Forchheimer terms) with additional terms for transitional flow and transient flow (implemented directly in Eq. 3). For generation and absorption of water waves, the *waves2Foam* library (Jacobsen et al., 2012) is used.

For the validation, the problem of transient flow past a porous block filled with rocks or beads presented by (Liu et. al, 1999) as reported in (Lin, 2008). This benchmark is used, here, to validate and test the different implemented seepage models. The case consists of a vertical column of crushed stones ($n = 0.49$, $D_{50} = 1.59$ cm.) of 30 cm breadth in the middle of a fish tank. Water is retained on the left basin by a vertical gate for a head of 23.85 cm then the gate is lifted to unleash the water to hit the crushed stone and flow to the other side. The fish tank extends 30 cm on both sides of the crushed stones column. Results from the numerical simulations for different seepage models against experimental results are shown in Figure 1.

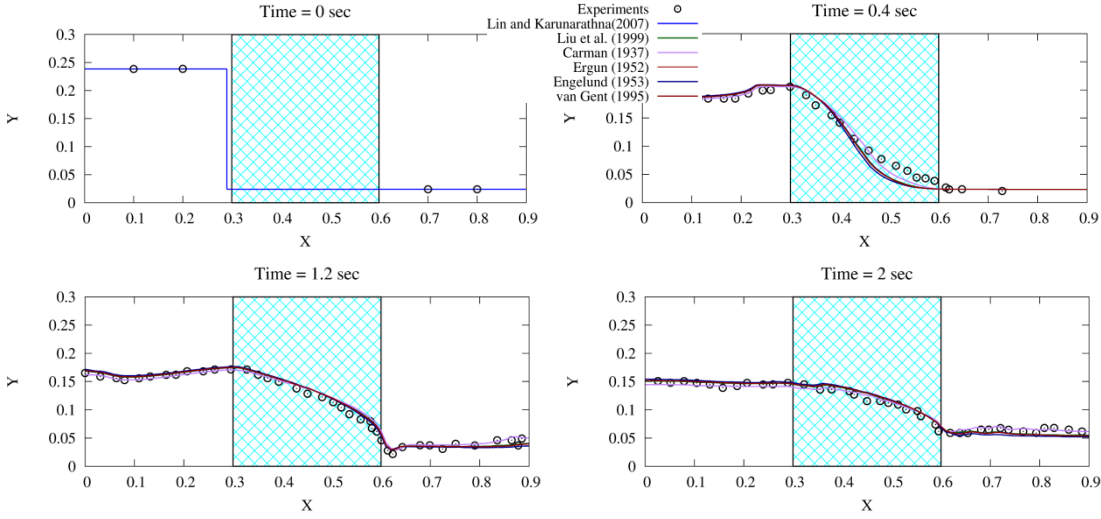


Figure 1. Porous dam break for different seepage models (porous media hatched)

3 THE GEOTECHNICAL MODEL

Modelling the seabed as a porous medium is essential to reproduce the strong interaction between the skeleton and the pore fluid. Biot's fully-coupled fully-dynamic formulation is the most widely applied in geotechnical engineering, especially by using the physical approach to the formulation provided, which is used in this study. The governing equations are: (1) Overall equilibrium equation for the solid-fluid mixture:

$$\nabla \cdot \boldsymbol{\sigma} - \rho \frac{\partial^2 \mathbf{u}}{\partial t^2} - C \frac{\partial \mathbf{u}}{\partial t} - \rho_f \left(\frac{\partial \bar{\mathbf{U}}}{\partial t} + \bar{\mathbf{U}} \cdot \nabla \bar{\mathbf{U}} \right) + \rho \mathbf{b} = 0 \quad (6)$$

Where $\boldsymbol{\sigma}$ is the total stress tensor, \mathbf{u} is the displacement vector and $\bar{\mathbf{U}}$ is the average Darcy's velocity vector of the percolating fluid. The third term in the left hand side of Eq. 6 represents the pore fluid acceleration relative to the solid phase. The underlined term represents convective pore fluid acceleration. Further, (ρ_f) is the density of the fluid, $\rho \mathbf{b}$ is the body force per unit mass tensor (mostly due to gravity, \mathbf{b} = gravitational acceleration), C is the attenuation (damping) coefficient and ρ is the density of the mixture defined as: $\rho = n\rho_f + (1-n)\rho_s$, where (ρ_s) is the solid particles density and (n) is the porosity. In Eq. 6, the stress is defined in a generic incremental fashion that permits the implementation of constitutive model for any material as $\boldsymbol{\sigma} = \boldsymbol{\sigma}' - p\mathbf{I}$ (tensile stresses are positive) and $d\boldsymbol{\sigma}' = \mathbf{E} : d\boldsymbol{\varepsilon}^e$, where $\boldsymbol{\sigma}'$ is the *effective* stress tensor and \mathbf{E} is the elasticity tensor and \mathbf{I} is the identity tensor. The strain-displacement relationship is considered for the assumption of small-strain.

(2) Momentum balance of the fluid phase alone considering the same control volume and assuming that the solid phase to be the reference is written as:

$$-\nabla p - \mathbf{S} - \rho_f \frac{\partial^2 \mathbf{u}}{\partial t^2} - \rho_f \left(\frac{\partial \bar{\mathbf{U}}}{\partial t} + \bar{\mathbf{U}} \cdot \nabla \bar{\mathbf{U}} \right) / n + \rho_f \mathbf{b} = 0 \quad (7)$$

Where p is the pore pressure and \mathbf{S} is a sink term that represents the viscous drag force vector (resistance). The viscous drag force can be defined according to the Darcy seepage law assuming an isotropic medium as, where $\mathbf{S} = \bar{\mathbf{U}} \rho_f g / K$ K is the isotropic hydraulic conductivity (m/s). (3) Mass conservation of the fluid flow is defined as:

$$\nabla \cdot \bar{\mathbf{U}} + \frac{\partial \varepsilon_v}{\partial t} + \frac{1}{Q} \frac{\partial p}{\partial t} = 0, \quad (8)$$

where $\varepsilon_v = tr(\boldsymbol{\varepsilon})$ is the volumetric strain of the solid skeleton. In addition to the fully dynamic fully coupled Biot's equations, the u - p approximation to the governing equations is implemented in which the pore fluid acceleration is completely neglected and the pore fluid momentum balance equation is not solved and hence the set of governing equations is reduced to: (1) Mixture momentum balance:

$$\nabla \cdot \boldsymbol{\sigma} - \rho \frac{\partial^2 \mathbf{u}}{\partial t^2} + C \frac{\partial \mathbf{u}}{\partial t} + \rho \mathbf{b} = 0 \quad (9)$$

and (2) Pore fluid mass balance:

$$\nabla \cdot \left(\frac{K}{\rho_f g} \left(-\nabla p - \rho_f \frac{\partial^2 \mathbf{u}}{\partial t^2} + \rho_f \mathbf{b} \right) \right) + \frac{\partial \varepsilon_v}{\partial t} + \frac{1}{Q} \frac{\partial p}{\partial t} = 0 \quad (10)$$

The developed geotechnical solver (*geotechFoam*) uses a segregated algorithm for solving the coupled equations using the finite volume method with traction correction at multi-material interfaces. The segregated approach uncouples the equations at the iteration level. The governing equations are discretized into implicit terms, which are used for solution of current iteration, and explicit terms, which are updated from the previous iteration. The (u - p) approximation is implemented in a straightforward manner. Nonetheless, the fully dynamic formulation need an approach to resolve the velocity-pressure ($\bar{\mathbf{U}}$ - p) coupling for the pore fluid. The same problem exists for CFD models. Therefore, the PISO algorithm (Pressure Implicit with Splitting of Operators) is adapted from CFD solvers to solve the momentum balance and diffusion equations for the pore fluid. For the structure-soil interface, a contact model was implemented which can simulate the separation and reattachment of soil and structure adjacent surfaces. The contact also accounts for friction between caisson surface and sand foundation. The non-linearity of the system is caused by the fact that the boundary condition is solution-dependant. A mixed boundary condition (*Dirichlet-Neuman*) is defined for the displacement at the contact boundary. A fixed value (*Dirichlet*) is used for displacement component normal to contact surface while a fixed displacement gradient (*Neumann*) is used for tangential components (friction). This mixed boundary condition is defined for the surface normal. Three values are defined: (i) the displacement, (ii) the displacement gradient and (iii) the value-fraction to define which part of the boundary is in contact and consequently which fraction of the displacement value and gradient is assigned for the calculation. Different (potential) pairs of contact surfaces are defined by the user and one of them is assigned a mixed boundary condition and the other is assigned a fixed-gradient boundary condition. Both boundaries are updated together when the contact surfaces overlap (during iterations). The normal contact constraint can be represented as:

$$g_n = 0, \text{ when } \sigma'_n > 0; \quad g_n > 0, \text{ when } \sigma'_n = 0; \quad g_n \sigma'_n = 0 \quad (11)$$

where g_n is the relative displacement in normal direction (separation) and σ_n is the normal stress component. The contact adopts Coulomb's law of friction for tangential constrains, as:

$$g_t = 0, \text{ when } \mu \sigma'_n - |\sigma_t| > 0; \\ |g_t| > 0, \text{ when } \mu \sigma'_n - |\sigma_t| = 0; \quad g_t (\mu \sigma'_n - |\sigma_t|) = 0 \quad (12)$$

where g_t is the relative displacement in tangential direction (slide). The tangential stress at contact is σ_t and the coefficient of friction is μ . No adhesion is simulated by the contact.

Modelling the soil foundation as a continuum dictates the introduction of a material constitutive model for the solid phase of soil (i.e. the skeleton). Implementing simple material models (e.g. linear elasticity) in a fully coupled and fully dynamic poro-mechanical model can only reproduce the transient pore pressure in the soil. To model residual pore-pressure accumulation underneath monolithic structures, the residual deformation of soil must be accounted for. Classical elasto-plastic models (where an elastic region of soil behaviour is enclosed by a plastic yielding envelope) are capable of reproducing soil behaviour when subject to monotonic loading. Nevertheless, in case of cyclic loads (especially with small amplitudes) classic elasto-plastic models tend to behave like elastic models (with load fluctuations occurring inside the elasticity region). Therefore, more sophisticated material constitutive models are needed to capture plasticity due to small changes in load-time history.

Unfortunately, no soil constitutive model exists, yet, that can be considered as a standard for soil dynamic analysis. Nevertheless, several promising models exist with advantages and disadvantages in reproducing behaviour of soil under specific conditions. Densification models decouple the soil strain into monotonic part and a densification part (damage) caused by cyclic loading. Densification models are relatively simple but may suffer on the accuracy side. Multi-yield surface (kinematic) models approximate the stress-strain curve for soil into small linear segments. Bounding surface models use only two surfaces from which the inner surface can translate inside the outside "failure" surface eliminating the need for

other yield surfaces and reducing calculation time. Some other models need no explicit definition of a yield (failure) surface like the generalized plasticity and hypoplastic models.

An interface for material models implementation in the *geotechFoam* solver has been developed. Different material models can be considered simultaneously for different regions of the domain. A multi-surface plasticity model (Elgamal, 2003) has been implemented in the *geotechFoam* solver. The model uses an incremental stress-strain relationship so Hooke’s law applies. The strain is conveniently decomposed into elastic and plastic components.

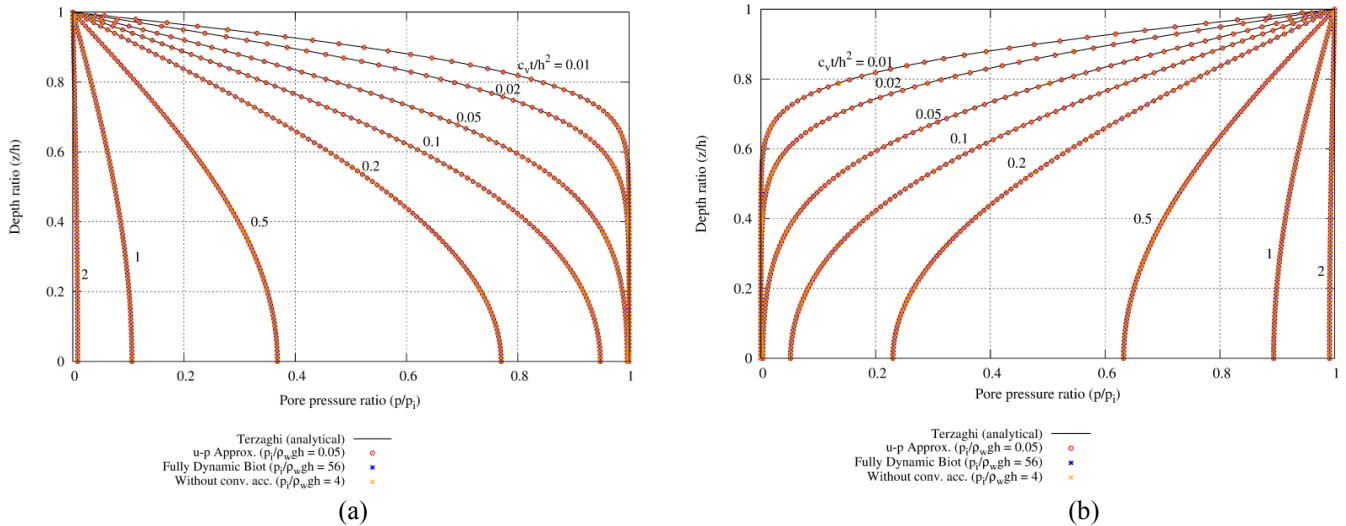


Figure 2. Comparative analysis of the three approaches with Terzaghi’s 1D consolidation model ($S = 98.83\%$): (a) Consolidation of a soil layer and (b) Loading by fluid

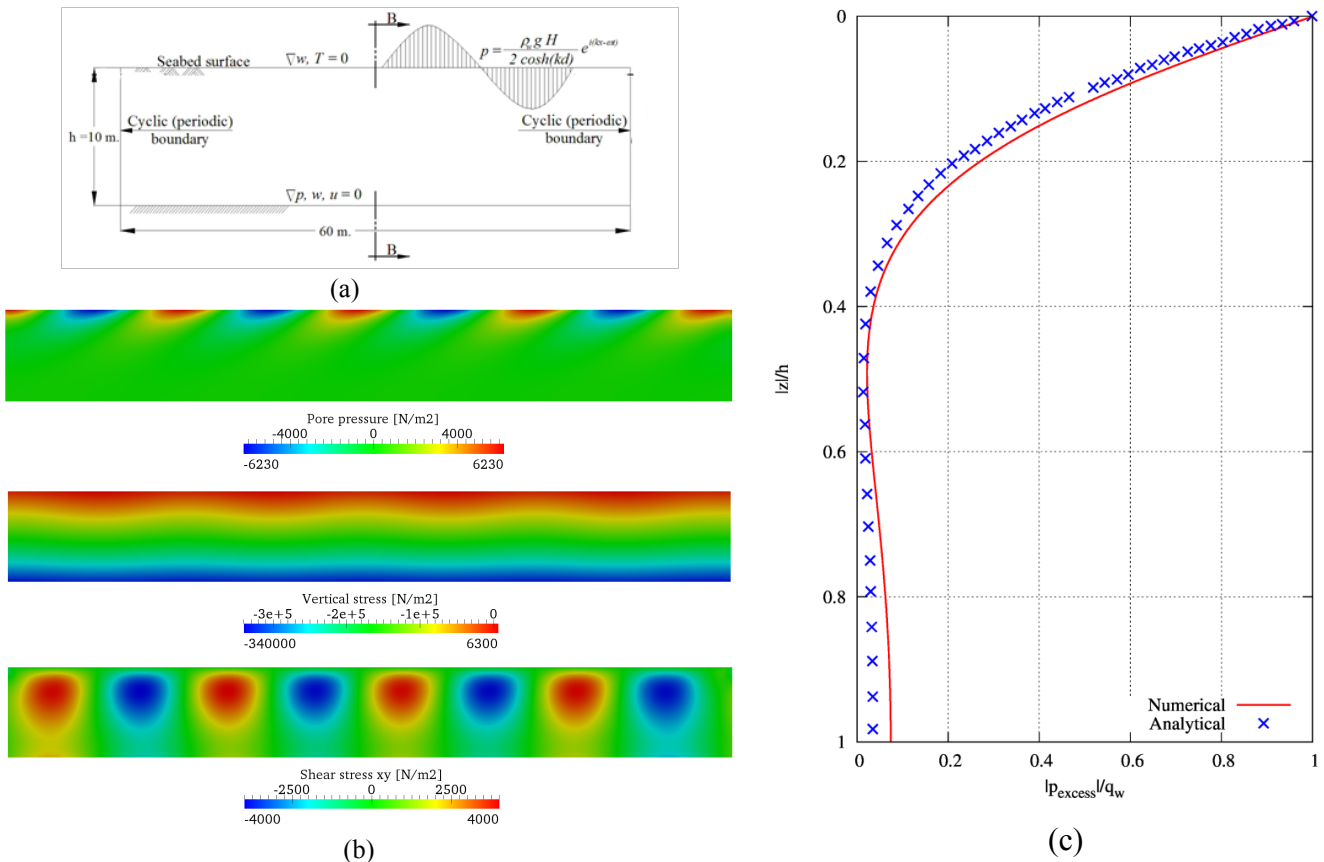


Figure 3. Seabed subject to direct wave action (no structure): (a) Computational domain, (b) Results of simulation, pore pressure, vertical soil stresses and shear stress (σ_{xy}) and (c) Pore pressure section (B-B) against solution of Jeng and Hsu (1996)

To verify the solid-fluid coupling, the analytical solution of Terzaghi’s one-dimensional consolidation of a soil layer is considered, which represents an uncoupled quasi-static solution. In this problem, the soil is initially considered undrained with an internal pore pressure dependent on the external uniform surcharge

and pore fluid compressibility; afterwards the soil is allowed to drain upwards from the surface. The solution can be adjusted to describe the accumulation of pore pressure as a result of the sudden loading by a fluid on the soil surface. In the second problem the initial pore pressure is set to zero and the fluid pressure at the surface is set to an arbitrary value. Figure 2 shows the results from different formulations as compared to Terzaghi's analytical solution. Numerical and analytical solutions agree very well.

Further, the effect of wave loading on an elastic seabed is studied using the three approaches (the fully dynamic solution, neglecting pore pressure convective acceleration and the $u-p$ approximation). The configuration of the problem is shown in Figure 3a. In Figure 3b, the excess pore pressure, vertical and shear stresses in the seabed are illustrated. The excess pore pressure ratio (pore pressure to wave pressure amplitude q_w) in the horizontal section (B-B) is compared to the analytical solution from Jeng and Hsu (1996) in Figure 3c.

The experiments by Sumer et al. (2008) are considered to the capability of the model to reproduce buildup and subsequent dissipation of pore pressure and accompanied soil compaction. The experiments were developed for use in numerical models' validations (i.e. foundations of caisson breakwater). Nevertheless, relevant soil properties were not measured before the tests and therefore the results can be used for qualitative rather than quantitative validation. The numerical model results (Figure 4), show that the model succeed in reproducing the build up of pore pressure then the dissipation (although the load of the rocking plate continues throughout the test) due to soil compaction.

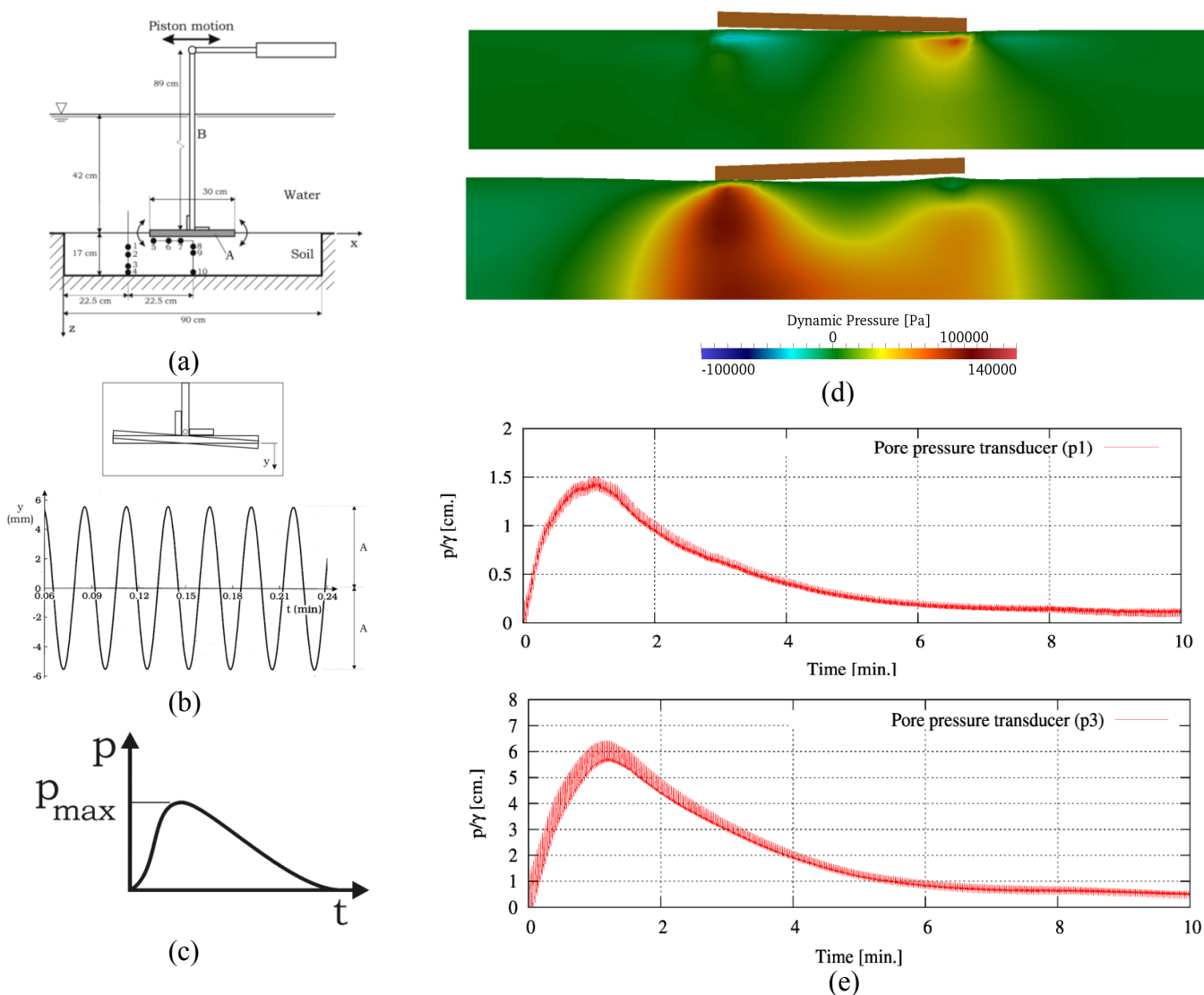


Figure 4. Physical tests of a forced rocking plate on a sand box: (a) test setup, (b) sketch of applied plate rocking motion, (c) a sketch of typical results of excess (residual) pore pressure at any given point (Sumer et al., 2008). (d) Computed excess pore pressure ($t = 1$ and $t = 30$ s.) and (e) probes of excess pore pressure at points 1 and 3 inside the sand box

4 LARGE-SCALE CAISSON BREAKWATER TESTS

The model tests were performed in the Large Wave Flume (GWK) in Hanover (Figure 5a). The effective length of the flume is about 307 m, the width 5 m and the depth 7 m. The wave paddle is driven by an engine with a maximal power of 900 kW. After a horizontal bottom of 250 m the flume is limited by an impermeable embankment with a slope of 1:6. The investigated model construction includes the sand body beneath the breakwater, the rubble foundation with a seaward berm and the caisson breakwater [29]. In Figure 8, the array of different wave gauges is shown. As shown in Figure 5b, the caisson structure was fitted with wave pressure transducers as well as displacement meters at the top of the caisson to measure its rigid body motion. Several pressure transducers were positioned on a wooden frame that is buried inside the sand foundation to measure pore pressure inside the sand foundation.

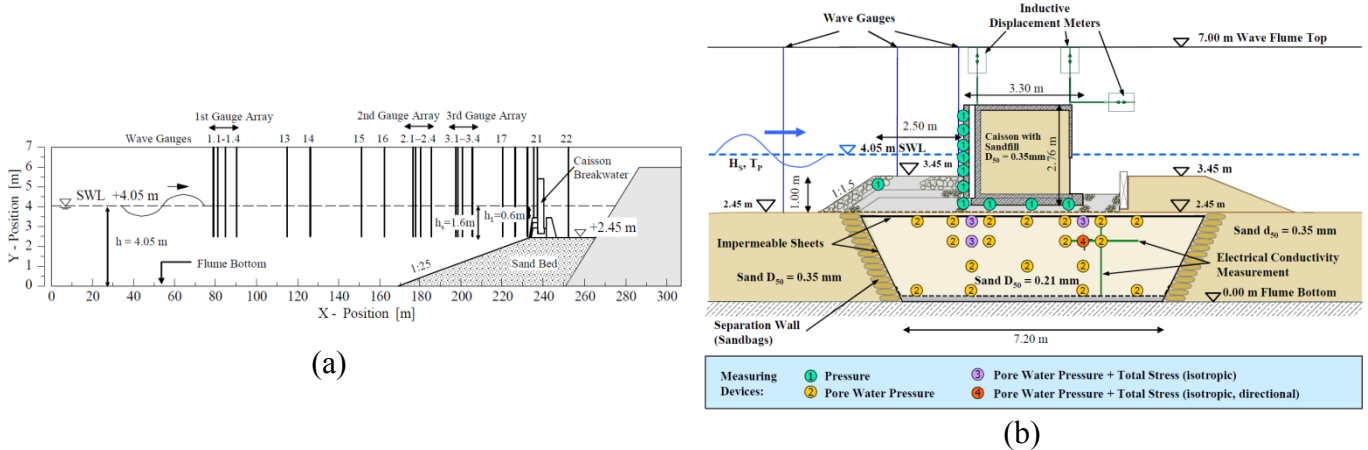


Figure 5. Caisson breakwater model set-up: (a) locations of wave gauges in the Large Wave Flume and (b) Cross section of the caisson and foundation model with locations of measuring devices (Oumeraci and Kudella, 2004)

Results from the hydrodynamic model are presented for three test cases of the large-scale caisson breakwater experiments with regular waves: non-breaking waves ($H = 0.4$ m. and $T = 5.5$ s.), slightly breaking waves ($H = 0.5$ and $T = 6.5$ s.) and breaking waves ($H = 0.7$ m. and $T = 6.5$ s.). The experimental results were not filtered from noise in measured signal. Results of wave pressure on the caisson breakwater are shown in Figure 6. The results agree quite well for the three wave types. The introduction of the compressibility term to the continuity equation (Eq. 1) enhances the results of the breaking wave impact by producing oscillation in pressure after the impact. This behaviour is observed in physical experiments and is justified by the oscillation of trapped air inside the breaker and cannot be reproduced by incompressible hydrodynamic models. Results of the pore pressure inside the rubble foundation show good agreement with physical test results as well. However, for the uplift pressure on the caisson (Figure 6e), the computed uplift pressure is of higher amplitude compared to the measurements. This is partially due to the fact that uplift pressure on caisson structures is affected by its motion (Oumeraci et al., 2001). This effect is magnified because of the impermeable sheet underneath the caisson, which is non-deformable in the hydrodynamic model while it actually has a response to change in pore pressure. It is anticipated that introduction of mesh motion to the hydrodynamic model (as feedback from the structural model) would enhance the results and reduce computed uplift pressure amplitude. The caisson idealized geometry with considered boundary conditions, domain discretization and deformed mesh are shown in Figure 7.

5 SUMMARY AND CONCLUDING REMARKS

A one-way coupled CFD-CSD model system is developed using the OpenFOAM® framework. The model system uses a one-way weak coupling approach between the developed geotechnical model (CSD) and the developed hydrodynamic model (CFD). The geotechnical model uses the PISO algorithm for solving the fully dynamic fully coupled Biot's equations. The fluid momentum balance is solved in the PISO based approach instead of being considered implicitly in the mass conservation equation in other approaches. Hence, the PISO based model calculates the total pore pressure instead of calculating the excess pore pressure in other approximations.

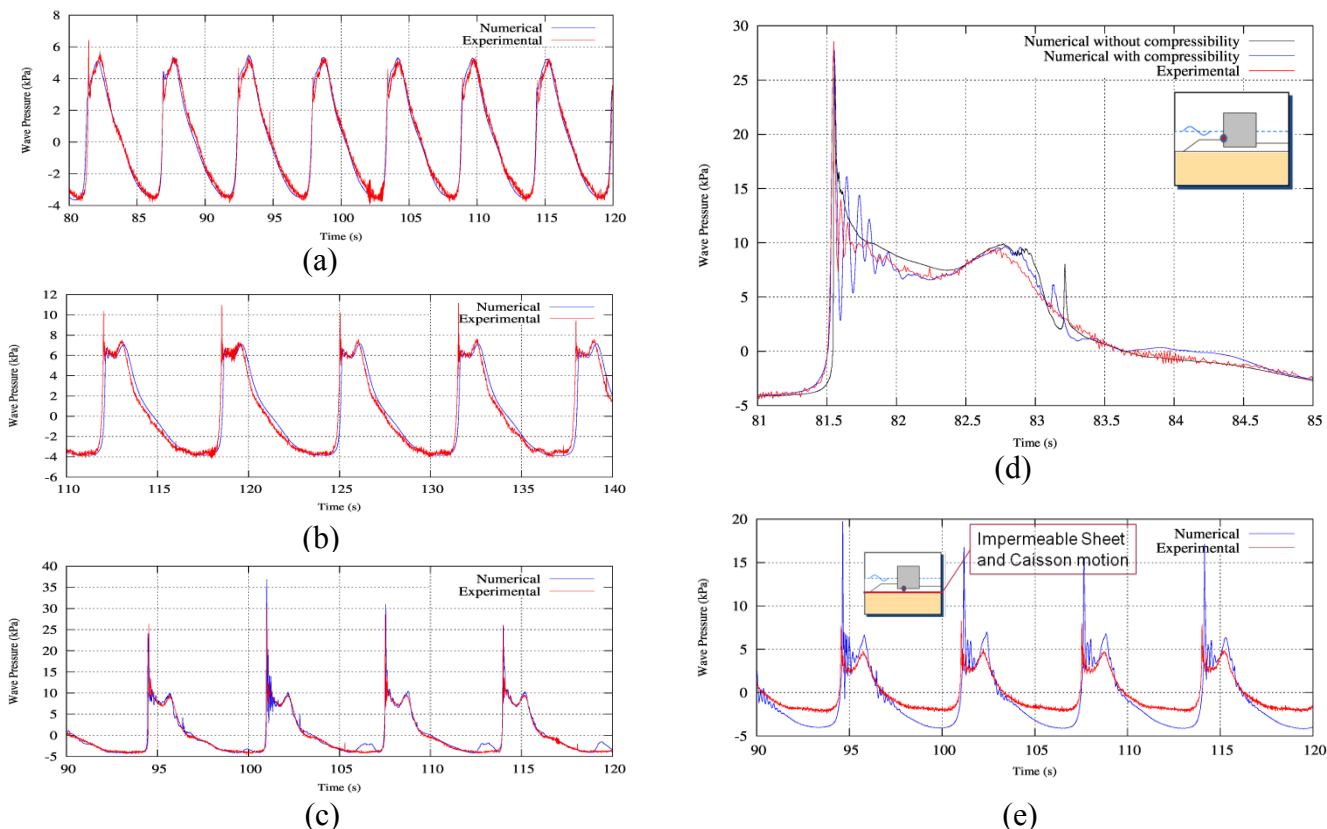
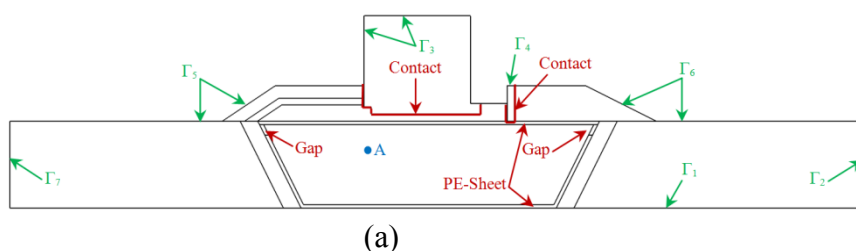
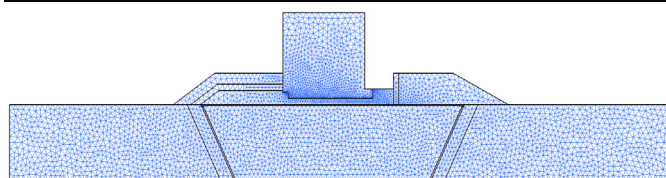


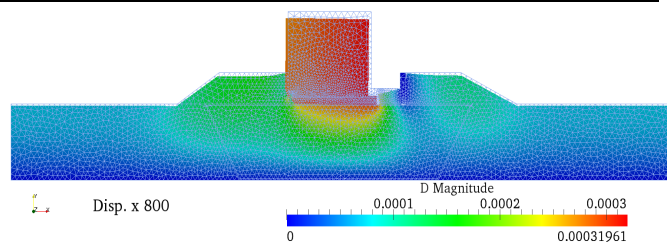
Figure 6. Wave pressure on the caisson breakwater face: (a) non-breaking waves ($H = 0.4$ m. and $T = 5.5$ s.), (b) Slightly breaking waves ($H = 0.5$ m. and $T = 6.5$ s.), (c) Breaking wave impact ($H = 0.7$ m. and $T = 6.5$ s.), (d) breaking wave impact single event (incompressible vs. compressible fluid) and (e) uplift pressure on caisson breakwater (breaking wave).



	Description	u	p	\bar{U}
Γ_1	Bottom of geometry	$u = 0$ - "Fixed bottom"	$\nabla p = 0$	$\bar{U} = 0$
Γ_2	Right side of geometry	Mixed - "Allows vertical settlement"	$\nabla p = 0$	$\bar{U} = 0$
Γ_3	Caisson top and seaward side	Input traction (from CFD)	$p = 0$	$\bar{U} = 0$
Γ_4	Top and left side of shutter beam	$u = 0$	$p = 0$	$\nabla \bar{U} = 0$
Γ_5	Rubble and seabed surface seaside	Zero traction	Value (from CFD)	$\nabla \bar{U} = 0$
Γ_6	Other outer boundaries	Zero traction	$p = 0$	$\nabla \bar{U} = 0$
Γ_7	Left side of geometry	Mixed - "Allows vertical settlement"	Value (from CFD)	$\nabla \bar{U} = 0$
	Contact	Contact boundary condition (mixed Dirichlet-Neumann)	Value (from CFD)	$\nabla \bar{U} = 0$



(b)



(c)

Figure 7. (a) Idealized geometry for the caisson breakwater and its foundation as tested in GWK, (b) domain discretization and (c) deformed mesh for caisson breakwater test

It is further observed that for the fully dynamic model the generation/dissipation of excess pore pressure is affected by the ratio of the excess pore pressure to the hydrostatic pore pressure. Further, the air content in the pore fluid (fluid compressibility) significantly affects the results. Neglecting convective acceleration of the pore fluid does not yield any computational benefit.

Different material models can be explicitly introduced into the model. A multi-surface plasticity model is implemented to reproduce the behaviour of sand foundation under cyclic loading induced by caisson motions. The use of the elastic-plastic model enables the successful simulation of pore pressure accumulation (build-up) and dissipation. Further, a frictional contact model is implemented in the solver to simulate soil-structure interaction.

The hydrodynamic model is developed for simultaneous solution of flow inside and outside the porous media using the principle of velocity averaging and an advanced seepage model. Adding change of fluid volume due to pressure change has improved results of breaking wave impact on the structure.

ACKNOWLEDGEMENT

Financial support of both the Egyptian ministry of higher education and the German Academic Exchange Service (DAAD) for the first author doctoral studies is gratefully acknowledged.

REFERENCES

- Elgamal, A., Yang, Z., Parra, E., and Ragheb, A., 2003, "Modeling of Cyclic Mobility in Saturated Cohesionless Soils", *International Journal of Plasticity*, Pergamon, Elsevier Science Ltd., Vol. 19, Issue 6, pp. 883-905.
- Jacobsen, N. G., Fuhrman, D. R., and Fredsøe, J., 2012. "A Wave Generation Toolbox for the Open-Source CFD Library: OpenFoam®". *Int. J. Numerl. Meth. Fluids*, **70(9)**, pp. 1073–1088.
- Jeng D.-S., Hsu J.R.C., 1996. "Wave-induced soil response in a nearly saturated seabed of finite thickness". *Geotechnique* **46(3)**,427-40.
- Kudella, M., Oumeraci, H., de Groot, M.B. and Meijers, P., 2006, "Large-Scale Experiments on Pore Pressure Generation underneath a Caisson Breakwater", *Journal of Waterway, Port, Coastal, and Ocean Engineering*, Vol. 132, No. 4, pp. 310-324.
- Lin, P., 2008, "Numerical Modeling of Water Waves, an Introduction for Engineers and Scientists", Taylor & Francis., New York, USA
- Oumeraci, H. and Kudella, M., 2004, "Liquefaction around marine structures (LIMAS) – Work package 3, large scale experiments on a caisson breakwater", *Technical report of Leichtweiß-Institute for Hydraulic Engineering and Water Resources, TU Braunschweig*, Braunschweig, Germany, 119 pp.
- Sumer, S. K., Sumer, B. M., Dixen, F. H. and Fredsøe J., 2008, "Pore Pressure Buildup in the Subsoil Under a Caisson Breakwater", *Proceedings of the Eighteenth (2008) International Offshore and Polar Engineering Conference*, Vancouver, BC, Canada, July 6-11
- Ülker, M.B.C., Rahman, M.S. and Guddati, M.N., 2012, "Breaking wave-induced response and instability of seabed around caisson breakwater", *Int. J. Numer. Anal. Meth. Geomech.* 2012; Vol. 36: 362–390.